Multipath Characteristics of Non-specular Wave Scattering from Building Surface Roughness

Hary Budiarto*, Kenshi Horihata*, Katsuyuki Haneda† and Jun-ichi Takada†
*Dept. of Electrical and Electronic Engineering
Tokyo Institute of Technology, 2-12-1 O-okayama Meguro-ku JAPAN 152-8552
Email: hary@mobile.ss.titech.ac.jp
†Dept. of International Development Electrical Engineering
Tokyo Institute of Technology, 2-12-1 O-okayama Meguro-ku JAPAN 152-8552
Email: haneda@mobile.ss.titech.ac.jp, takada@ide.titech.ac.jp

***Abstract*— This paper presents multipath characteristics of non-specular scattering from building surface roughness. Superresolution method was applied as an approach to handle signal parameters (DOA, TOA) of the individual incoming waves reflected from building surface roughness. In order to comprehend in detail the microscopic mechanisms of scattering, signal parameters are to be incorporated into the geometrical ray tracing. The results show that the multiple paths can be detected from many scatterers, such as ground, window glass, window frame, bricks surface, as well as directly from the transmitter. Most of the scattered waves arrives closely from specular directions.**

I. Introduction

Wireless personal communication system has been continuously developed world wide. The main aim of the development is to pursue better services with higher data transmission rate. The system has also been extended to new complex environments, such as urban and indoor microcells. In urban area, buildings are the dominant scatterers determining propagation properties. Reflection, diffraction, transmission and scattering of the electromagnetic waves on the building surfaces in the radio environment give rise to multipath propagation. Consequently, the transmitted signal reaches the receiver through different propagation paths. Multipath prediction on a building surface was conventionally based on an assumption that reflection from the surface has a substantial specular direction [2][3][4]. However, the multiple paths are also generated by scattered wave propagating in non-specular direction. Therefore, non-specular scattering from the building surface can affect the channel characteristics as well as specular scattering [1]. In order to predict channel characteristic in more detail, the multipath propagation of microscopic scattering are important. This paper presents multipath characteristics of non-specular wave scattering from building surface roughness based on the experimental results. The antenna element was scanned spatially to detect the directions of arrivals (DOA) and the carrier frequency was scanned to obtain the times of arrivals (TOA). A super resolution method was applied as an approach to handle the signal parameters (DOA, TOA) of the individual incoming waves scattered from building surface roughness. In order to comprehend the microscopic mechanism of scattering, the signal parameters are to be incorporated into the geometrical ray-tracing. Two models of the spatial scanning were applied to predict multipath characteristics in more detail. The result shows that the multipath propagation can be detected from many scatterers, such as ground, window glass, window frame, bricks surface, as well as directly from transmitter. The parameters of the arrival wave from the building scatterer have a tendency to be distributed around the angle of specular direction.

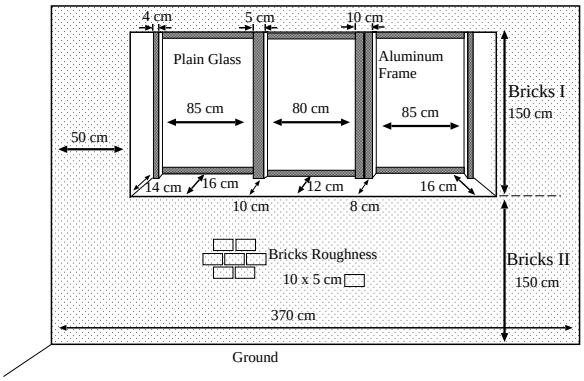

Fig. 1. Building Surface Profile

II. Environment Under Consideration

A. Building Surface Profile

Profile of the building surface is shown in figure 1. The profile was taken from one of the buildings in Tokyo Institute of Technology. The surface of the building has non-uniformity due to the windows (glass), frames (aluminum), and wall (bricks). The surface has periodical irregularity. One period of the surface equals 3.7 m. The windows are made up of the sidewall, aluminum frames and plain glasses, which in principle are the building roughness, besides the wall surface itself. The window's glasses of the building are of three different dimensions as follows: 85x150 cm, 80x150 cm, and 85x150 cm respectively. Accordingly, the aluminum frames are located between the first window with sidewall, the first window and the second window, and between the second

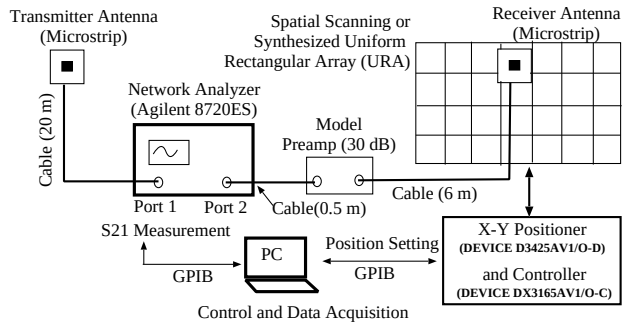

Fig. 2. Equipment Arrangement

windows with the third window. Outer dimensions of the aluminum frames are 4x150 cm, 5x150 cm and 10x150 cm. The first window glass and frame has the same offset depth of 16 cm with the third one. However, the second window glass and frame are 4 cm more protruding from the others. The windows are 1.5 meter from the ground. The wall surfaces are made of bricks that have periodical roughness in horizontal and vertical directions with dimension of 10x5 cm with interval 1 cm.

B. Transmitter and Receiver Models

Transmitter and receiver antennas were linearly polarized rectangular microstrip antennas with the ground plane size of 8 by 8 cm. The patch size was 1.79 by 1.79 cm on dielectric substrate with $\epsilon_r = 2.55$. Center frequency of the antennas was 4.95 GHz with bandwidth of 180 MHz. The wavelength was comparable with or smaller than depth of building surface roughness. The receiver antenna was shifted spatially by X-Y positioner to obtain field strength at each point in the scanning region. The height of transmitter antenna was 1.9 meter from ground. The transmitter antenna was fixed at 2.7 m away in front of the building surface. Both antennas were aligned to transmit and receive vertical polarization. The transfer function between transmitter and receiver antennas were measured using vector network analyzer (VNA).

Figure 2 shows equipment arrangement of the experiment. Measurement of transfer function and the shifting of receiver antenna are operated automatically using personal computer through the positioner controller and General Purpose Interface Bus (GPIB) to achieve high accuracy. The X-Y positioner is used for automatically shifting the receiver antenna with accuracy of 1 mm. All of the experimental parameters are presented in table 1.

C. Calibration System

Since the VNA measured transfer function of the cable and amplifier simultaneously, a calibration of the data measurement system was required to eliminate the effect of equipment. The transfer function can be expressed as follows,

$$X(f) = H(f) \times G(f) \tag{1}$$

TABLE I

EXPERIMENTAL PARAMETERS

Antennas	Tx & Rx Microstrip Reflection coefficient is bellow -10 dB in 4.85 - 5.05 GHz.
Measurement Points	Spatially 10 $\times$10 points (25 mm interval), 21 points over frequency (4.85 - 5.05 GHz).
Snapshot	20 times
Estimated Parameters	The number of waves and each wave's azimuth, elevation, delay and path gain
Signal Processing	LS 3-D Unitary ESPRIT
Smoothing in ESPRIT	Spatially 4 times and 7 times over frequency
Wave Polarization	Vertical-Vertical
Normalization	Face-to-face, the distance between Tx and Rx is 1 m at experiment location

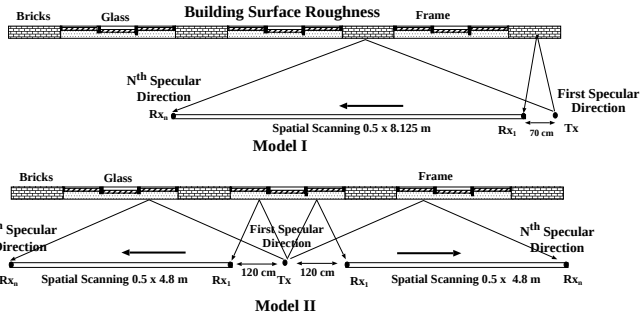

Fig. 3. Top View of the Spatial Scanning Model

where $G(f)$ is transfer function of the cable, amplifier and antenna complex directivity, and $H(f)$ is Friis's free space transfer function, which is given as,

$$H(f) = \frac{\lambda}{4\pi d} \exp(-j\frac{2\pi}{\lambda}d) \tag{2}$$

where d is propagation path, and λ is wavelength. All measurement data resulted from this experiment were already calibrated applying $G(f)$ function, which is obtained from the measurement using the transmitter and receiver antennas positioned face-to-face with 1 meter distance to each other in an open space.

D. Spatial Scanning Model

The spatial scanning was configured to resemble an antenna array called synthesized uniform rectangular array (URA). The X-Y positioner was used for automatically shifting the receiver antenna in the scanning region. Measurement points during the spatial scanning were discretized for every 2.5 cm toward the horizontal and vertical directions. The measurement was performed along 50 cm in vertical direction. The middle of vertical direction scanning region is the same as the height

of transmitter antenna. Figure 3 illustrates two models of the spatial scanning. Model-I performs the measurement along 812.5 cm to horizontal direction. The transmitter antenna is positioned facing bricks surface of the building. The first vertical direction of measurement is 70 cm away from the transmitter antenna, which corresponds to 10° incident angle in specular direction. As for Model-II, the transmitter antenna is positioned facing glass surface of the building, with spatial scanning performed along 480 cm to horizontal direction. The first vertical direction of measurement is 120 cm away from the transmitter. The purpose of model-II is to observed in more detail the multiple paths effect characteristics affected by the changes in spatial scanning position and the direction of the incoming signal. This model performs the measurement at two different sides, which are from the left hand and from the right hand of the transmitter.

III. Signal Processing

In order to obtain signal parameter of the arrival wave, an expression of data measurement was formulated. Suppose that the L waves impinging at the receiver that have three parameters of azimuth angle ϕ_l, elevation angle θ_l and delay time τ_l, where $(1 \leq l \leq L)$. With X-Y positioner, the receiver antenna performs spatially scanning both in azimuthal and elevated directions where the intervals of the sampling points are Δ_x, and Δ_y. The numbers of sampling points are M_1 and M_2, respectively. At each sampling point, it carries out M_3 point of sampling over the frequency where the interval of sampling is Δ_f and the center frequency f_c. If the electrical length of the aperture size of array $\frac{2\pi}{\lambda}M_1\Delta_x$ or $\frac{2\pi}{\lambda}M_2\Delta_y$ is small enough to be assumed as constant within the bandwith $M_3\Delta_f$, i.e, $M_1\Delta_x \cdot M_3\Delta_f \ll c$, and $M_2\Delta_y \cdot M_3\Delta_f \ll c$, where c is a light velocity, the measured data y_{k_1,k_2,k_3} can be expressed as,

$$y_{k_1,k_2,k_3} = \sum_{l=1}^{L}\left[s_l \prod_{r=1}^{3} e^{j\mu_l^{(r)}}\right] + n_{k_1,k_2,k_3} \tag{3}$$

where $0 \leq k_r \leq (M_r - 1)$ $(1 \leq r \leq 3)$ indicates a location of each sampling point, n_{k_1,k_2,k_3} is a white Gaussian noise of zero mean, s_l is a complex amplitude of l-th wave at a reference point and $\mu_l^{(r)}$ is denoted by,

$$\mu_l^{(1)} = \frac{2\pi}{\lambda}\Delta_x \sin\phi_l \cos\theta_l \tag{4}$$

$$\mu_l^{(2)} = \frac{2\pi}{\lambda}\Delta_y \sin\theta_l \tag{5}$$

$$\mu_l^{(3)} = 2\pi\Delta_f\tau_l \tag{6}$$

These values include a parameter of incident waves so that the target is to obtain these L sets of 3-D mode parameters. Then vectorization of data measurement can be defined as,

$$\begin{aligned} y = [&y_{1,1,1}\ y_{2,1,1} \ldots y_{M_1,1,1}\ \ y_{1,2,1} \ldots \\ &y_{M_1,M_2,1}\ y_{1,1,2} \ldots y_{M_1,M_2,M_3}]^T \in C^M \\ &= \boldsymbol{A}\boldsymbol{s} + \boldsymbol{n} \end{aligned} \tag{7}$$

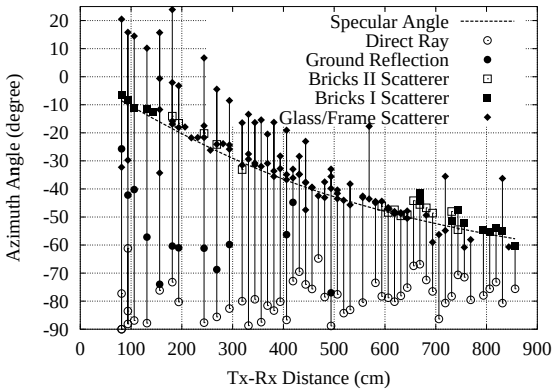

Fig. 4. Azimuth Angle of Arrival Wave from Scatterers

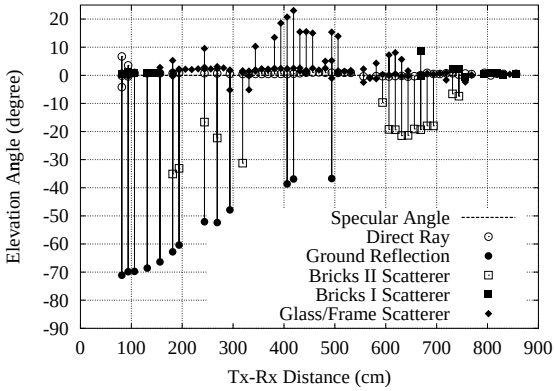

Fig. 5. Elevation Angle of Arrival Wave from Scatterers

where $s \in C^L$ and $n \in C^M$ $(M = M_1M_2M_3)$ are the complex amplitude vector and noise vector respectively. Then the multi-dimensional mode matrices $\boldsymbol{A} \in C^{M\times L}$ is expressed as (7) which is generated by mode matrices that correspond to each mode.

$$\boldsymbol{A} = \boldsymbol{A}(\mu^{(3)}) \diamond \boldsymbol{A}(\mu^{(2)}) \diamond \boldsymbol{A}(\mu^{(1)}) \in C^{M\times L} \tag{8}$$

$$\boldsymbol{A}(\mu^{(r)}) = [\boldsymbol{a}(\mu_1^{(r)}) \ldots \boldsymbol{a}(\mu_L^{(r)})] \in C^{M_r\times L} \tag{9}$$

$$a(\mu_l^{(r)}) = [1\ e^{-j\mu_l^{(r)}} \ldots e^{-j(M_r-1)\mu_l^{(r)}}]^T \in C^{M_r} \tag{10}$$

where $\diamond$ denotes the kronecker product of each row of the matrices. The 3D unitary ESPRIT [5][6][7] was used to obtain the signal parameter. It is a super resolution direction finding method of the arrival wave. In physical terms, the 3D unitary ESPRIT is equivalent to finding out the parameters of arrival wave by phase difference between groups of uniform positioned elements of sensor array. The ESPRIT matrix data had a size of (10×10) or (25×25) cm for each of observation point. The arrival wave analyses were performed at 60 observation points with an interval of 12.5 cm.

IV. Experimental Results

A. Directions of Arrivals Wave Profiles

Figure 4 shows the ESPRIT results for azimuthal angle of the arrival wave. The line perpendicular to x-axis depicts the

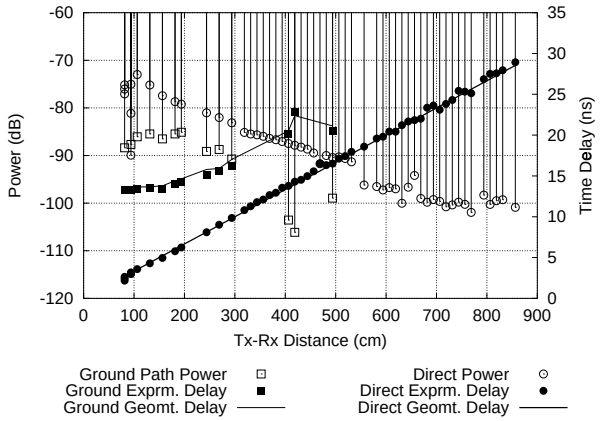

Fig. 6. Power and Time Delay of Arrival Wave for Direct and Ground Reflection

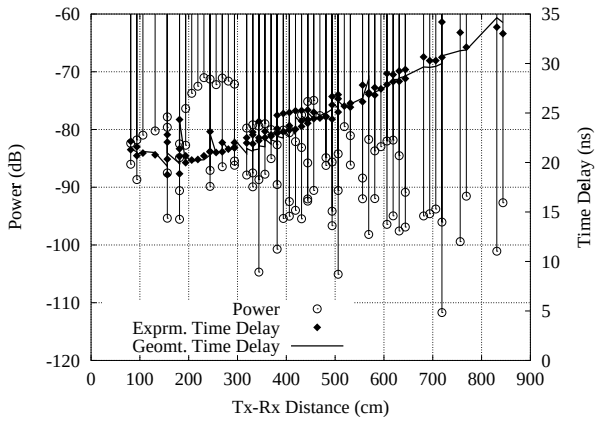

Fig. 7. Power and Time Delay of Arrival Wave for Windows Scatterer

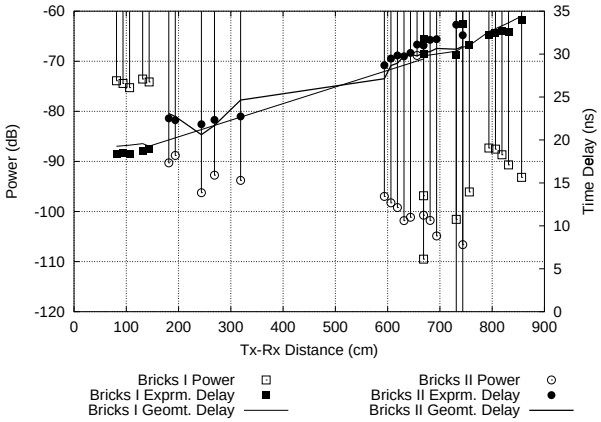

Fig. 8. Power and Time Delay of Arrival Wave for Bricks Scatterer

range of the azimuthal angle. Negative azimuthal angle means the wave is coming from the right-hand side of the receiver or source side (see figure 3).

The legends in figure 4 show the type of scatterers obtained from geometrical ray tracing. The number of icons on the vertical line corresponds to the number of multipath signals. Many scatterers can be detected such as from ground (solid circle), window glass & window frame (solid diamond), bricks-I surface (solid box), bricks-II surface (box) and directly from the transmitter (circle). The types of brick scatterer are distinguished between the bricks scatterer with the height between the lower and upper part of the windows, classified as bricks-I, and the bricks scatterer with the height below the windows, classified as bricks-II (see figure 1). The azimuthal angles of the building scattered are concentrated arround specular direction. Maximum deviation of the angle is 20°. Figure 5 shows elevation angle of the arrival wave. It can be seen that the value of elevation angle is around 0° for those arrival waves coming from windows and bricks-I scatterers. It implies that most of the scattered waves from building surface arrives closely from specular directions. Figure 5 also shows diffraction effect from windows frame when the distance between transmitter and receiver antenna was 350-500 cm or its specular point is located arround the center of windows. It is found when the arrival waves have large elevation angle. For instance, in the case of the first observation point located 81.25 cm from the transmitter, six (6) arrival waves were obtained, consisted of two waves that directly arrives, one ground reflection and three waves from building surface. The reason why that the two waves were directly obtained is because the distance between the transmitter and receiver is relatively close. Therefore, the receiver gets the reflection from support equipment of the antenna. This kind of result was only obtained at the first and second observation points.

B. Times of Arrivals Wave Profiles

The other parameters that can be obtained using ESPRIT are power and time delay. Figure 6 shows power and time delay of the arrival waves for direct and ground reflection paths. The comparison between time delay from the experiments and based on geometrical ray tracing are also presented. This figure shows that the arrival waves coming from the ground can be observed when the distance between transmitter and receiver antennas is less than 500 cm. The direct arrival wave is observed in all observation points. Figure 7 shows power and time delay of the arrival waves from the windows scatterer. This figure shows that more than one scattered wave from glass was found from every observation point. This is due to the refractory properties of the glass material and shape of the windows with higher roughness.

Figure 8 shows power and time delay of the arrival waves scattered from bricks. This figure shows that the power difference between bricks I and bricks II is significant compared with its delay difference even the are the same material. It is probable that this is caused by the reflection coefficient change due to the difference in elevation and roughness of the building.

The second order scattering was discovered from building scatterer when the delay obtained from the experiments is it longer than the delay of geometrical ray tracing and has low power. Figures 7 and 8 clarify that non-specular scattering from building surface is more dominated by window scatterers than brick scatterers. Figures 6, 7, and 8 show that the delay

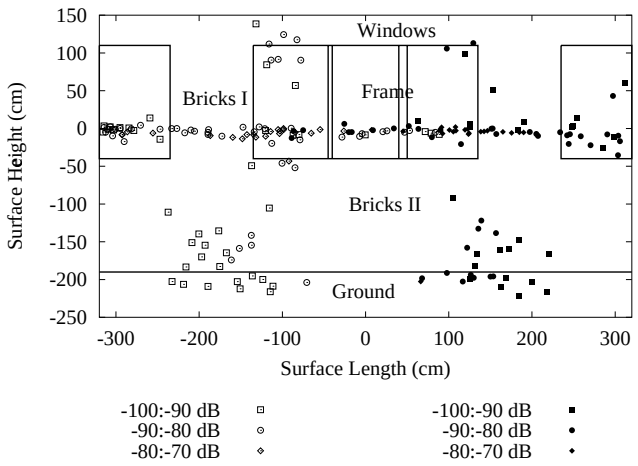

Fig. 9. Scattering Point for Model II of the Spatial Scanning

estimated using geometrical ray tracing corresponds to the experimental results. This implies that the classification of scatterer types shown in figures 4 and 5 are valid. The average of the differences between the delay of experimental and the delay of geometrical ray tracing-based are listed in table 2. The table shows that the average difference of experimental time delay with geometrical ray tracing time delay for the bricks and glass scatterer are larger than the others. The reason of these difference is that the time delay of the second order scattering is also included in the averaged calculated time delays.

TABLE II
AVERAGE DIFFERENCE OF EXPERIMENT TIME DELAY WITH GEOMETRICAL RAY TRACING TIME DELAY

Type of Scatterer	Difference
Direct	0.25 ns
Ground	0.38 ns
Bricks I	0.83 ns
Bricks II	0.51 ns
Glass	0.62 ns

C. Spatial Scanning Position Change

Figure 9 shows the scattering point profile of multipath propagation at the model II of the model II spatial scanning by comparing the power for each path. This figure shows that if the receiver is shifted from -120 cm to -300 cm, the dominant arrival waves arrive from the right hand side of the receiver and limited only by transmitter position. Likewise, if the receiver is shifted from 120 cm to 300 cm, the dominant arrival waves would come from the left hand side of the receiver and limited only by transmitter position. It was proven that multipath components are concentrated arround specular direction. The point at (0,0) coordinate is determined the transmitter position. The coordinates of the scattering points at the right and left hand side of the transmitter have similar characteristic, as well as the profile of its power. Figure 9 also shows diffraction effect from windows frame. It is found when arrivals wave have large elevation angle or coordinate of the scattering point was at the upper part of the windows.

V. CONCLUSION

This paper presents multipath characteristics of non-specular wave scattering from 3-D building surface roughness. The result shows that the multipath propagation can be detected from many scatterers, such as ground, window glass, window frame, bricks surface, as well as directly from the transmitter. The parameters of the arrival waves from the building surface have a tendency to be around the angle of specular direction. Maximum deviation of the angle is 20° in azimuth and elevation angle. The time delays can be correctly estimated using geometrical ray tracing. The second order scattering was observed from building surface. The non-specular scattering from building surface are more dominated by window scatterers rather than by brick scatterers.

Aknowledgement

The authors are really grateful to Professor H. Niiyama for the permission to use the GSIC-International Div. TIT building for our experimental purpose, This work is partly supported by JSPS Scientific Research Grant-in-Aid.

REFERENCES

[1] J. Takada, J. Fu, H. Zhu, and T. Kobayashi, “Spatio-Temporal Channel Characterization in a Sub-Urban Non-Line-of-Sight Microcellular Environment”, IEEE J. Select. Areas in Comm., vol. 20, no. 3, pp.532-538 Apr. 2002.

[2] H. Budiarto and J. Takada, “The Effect of Building Surface Roughness in Mobile Communication”,Proc. of Int. Symp. on Comm. Inf.Tech., pp.674-677, Thailand, 2001.

[3] M.O. Al-Nuami and M.S. Ding, “Prediction Models and Measurements of Microwave Signals Scattered from Buildings”, IEEE Transc. on Antenna and Propagation, vol.42, No.8 pp. 1126-1137 August 1994.

[4] A. Satoh and E. Ogawa, “An Evaluation Method for the Reflection Coeficient of Buildings Wall”, Electronics and Communications in Japan, Part 1, Vol. 73, No. 3, pp. 92-103 1990

[5] Haardt Martin and J.A. Nossek, “Simultaneous Schur Decomposition of Several Nonsymmetric Matrices to achieve Automatic pairing in Multidimensional harmonic Retrieval problems”, IEEE Transaction on Signal Processing Vol. 46 No. 1 pp. 161-169 January 1998.

[6] K. Sakaguchi, J. Takada, and K. Araki, “Multipath parameter estimation by using 3D Unitary ESPRIT”, IEICE Tech. Rep., AP98-35, June 1998.

[7] R. Roy and T. Kailath, “ ESPRIT- Estimation of Signal Parameters via Rotational Invariance Techniques”, IEEE Transc. on Acoustics, Speech and Signal Processing, vol.37, No.7, pp.984 -995, July 1994.